International Journal of Mineral Processing 98 (2011) 82–88

Contents lists available at ScienceDirect

International Journal of Mineral Processing

journal homepage: www.elsevier.com/locate/ijminpro

Electrochemical behaviour of chalcopyrite ($CuFeS_2$) in $FeCl_3$ solution at room temperature under differential stress

Qingyou Liu, Heping Li *

Laboratory for study of the Earth's Interior and Geofluids, Institute of Geochemistry, Chinese Academy of Sciences, Guiyang, 550002, China

ARTICLE INFO

Article history:
Received 28 January 2010
Received in revised form 14 April 2010
Accepted 20 October 2010
Available online 28 October 2010

Keywords:
Chalcopyrite
Polarisation curves
Electrical impedance spectroscopy
Differential stress

ABSTRACT

The electrochemical behaviour of chalcopyrite ($CuFeS_2$) was studied by polarisation curve and electrochemical impedance spectroscopy (EIS) in $FeCl_3$ solution at room temperature under differential stress. Experimental results showed the relation between chalcopyrite potential difference and elastic stress is $\Delta\varphi_H^{CuFeS2} = -\frac{VdP}{ZF}$. The corrosion current density and charge transfer electrical resistance increased distinctly, whereas double-layer capacitance decreased and the corrosion potential became more negative with increasing differential stress. The EIS data have been analyzed and discussed in the simple equivalent circuit model, the Randles equivalent electrical circuit model and the point defect model, respectively. The experimental results are significant for mineral processing and hydrometallurgy.

1. Introduction

As one of the most common sulphide minerals, the most abundant copper sulphide mineral, and the major commercial source of copper, chalcopyrite is broadly used in hydrometallurgy and mineral processing. Because chalcopyrite possesses the properties of a semiconductor, when oxygen and other oxidising ions are present, electrochemical oxidation may occur. These electrochemical oxidations often causes environmental concerns, such as dangers from heavy metals and acidic mine drainage. So there is a large amount literature devoted to electrochemical studies on chalcopyrite.

Previous electrochemical studies indicated that at different situations there have different outcomes. Some proposed the direct oxidation of chalcopyrite to Cu^{2+} and Fe^{2+} ions (Dutrizac and MacDonald, 1973; Munoz et al., 1979; Dutrizac, 1981; Hackl et al., 1995; Lu et al., 2000; Hiroyoshi et al., 2002): $CuFeS_2 \rightarrow Cu^{2+} + Fe^{2+} + 2S^0 + 4e^-$. Another study proposed the direct oxidation of chalcopyrite to covellite CuS (Gonzalo et al., 2007): $CuFeS_2 \Leftrightarrow 0.75CuS + 0.25Cu^{2+} + Fe^{2+} + 1.25S + 2.5e^-$. Still other studies proposed the formation of nonstoichiometric sulphides, $Cu_{n-1}Fe_{n-1}S_{2n}$, at the chalcopyrite electrodes (Price and Chilton, 1980; Lázaro et al., 1995; Arce and González, 2002): $nCuFeS_2 \Leftrightarrow Cu^{2+} + Fe^{3+} + Cu_{n-1}Fe_{n-1}S_{2n} + 5e^-$. In addition, when chalcopyrite is added to oxidation potentials' action, there may be various formations on the electrode. Vaughan et al. (1995), using electrochemical techniques and X-ray photoelectron spectroscopy, investigated the electrochemical oxidation of chalcopyrite ($CuFeS_2$) and its metal-enriched derivatives, haycockite ($Cu_4Fe_5S_8$), mooihoekite ($Cu_9Fe_9S_{16}$), and talnakhite ($Cu_9Fe_8S_{16}$). The results show that, at different electrode potentials, their relative rates of oxidation are in different order. Because chloride ions form complexes with Cu^+ ions and may act as bridges during electron transfers, a higher oxidation rate may be induced compared to other aqueous solutions. Velásquez et al. (1998) studied the $CuFeS_2$ electrode electrochemical behaviour by Electrochemical Impedance Spectroscopy (EIS) in alkaline solutions with different oxidation potentials. Their experimental results indicated that when V_{dc}<0.4 V versus saturated calomel electrode (SCE), the electrical equivalent circuit can be interpreted from a Randles model, and as a surface layer model when V_{dc}>0.4 V vs. SCE. Considering the variation of the charge-transfer electrical resistance of the redox reaction with the different applied DC potentials, the double-layer capacitance and other characteristic parameters, they determined that the variation is due to the initial formation of a layer of Fe_2O_3 and an inner layer of CuO and Fe_2O_3, which confers an irregular and non-homogeneous surface to the electrode. Lu et al. (2000) used carbon paste electrodes to study the electrochemical oxidation of chalcopyrite concentrate in a mixed chloride–sulphate electrolyte solution. Using both transient and steady state techniques, they demonstrated that, when chloride ions were present, the oxidation of the mineral was significantly enhanced. Farquhar et al. (2003) studied the electrochemical oxidation of chalcopyrite ($CuFeS_2$) at pH 4 using voltammetry, coulometry, X-ray photoelectron spectroscopy and both ex situ and in situ atomic force microscopy. The results demonstrated that chalcopyrite had an anodic oxidation peak between 500 and 650 mV prior to the onset of the main decomposition reactions. At 500 and 650 mV, the loss of Cu from the surface increases by a factor of two and six, respectively. Oxidation at

* Corresponding author.
E-mail address: liheping123@yahoo.com (H. Li).

0301-7516/$ – see front matter © 2010 Elsevier B.V. All rights reserved.
doi:10.1016/j.minpro.2010.10.010

500 mV resulted in the formation of a mixed oxide or hydroxide of iron, coincident with islands (<0.15 mm wide) of reaction products. The surface coverage of these islands increases with the amount of charge passed. The oxidation at 650 mV had similar processes with a greater island surface coverage and a more deeply altered surface.

In summary, the previous work on the electrochemical behaviour of chalcopyrite ($CuFeS_2$) is mainly focused on conditions without stress. However, whether the sulphide minerals are being exploited or simply experiencing geochemical processes, stress may act on them at all times. As a result of stress, strain energy changes into electrochemical energy, which changes the electrode potential, and thus has a major influence on the electrochemical behaviour of these sulphides minerals. On the other hand, as the most commonly used medium to leach sulphide (Dutrizac, 1992; Havlík et al., 1995), $FeCl_3$ has an important effect on the electrochemical behaviour of chalcopyrite. For the above reasons, the aim of this work was to study the electrochemical response of a massive chalcopyrite in $FeCl_3$ solution under differential stress in order to understand the differences in the dissolution kinetic and electrochemical mechanisms, and hence to provide the experimental basis for the mechanical activation of the chalcopyrite processing and hydrometallurgy.

2. Experimental methods

2.1. Preparation of the CuFeS2 electrode, reagents and instrumentation

A $CuFeS_2$ electrode was prepared from a dense, massive, natural chalcopyrite (origin: Daye mine, China); the sample was cut and shaped into a 10 mm × 10 mm × 40 mm block. The electron microprobe analysis confirmed the Fe, Cu and S contents (wt%) as 30.70%, 34.04% and 34.67%, respectively. Before the experiments, fresh electrode surface was prepared using 1#–5# SiC abrasive paper, cleaning with filter paper and rinsing with acetone until clean. After each experiment, the used chalcopyrite electrode was repolished and reused.

Electrolytes were prepared from analytical grade chemicals and doubly distilled water containing various concentrations of $FeCl_3$. During all of the experiments, the electrochemical cell, which we made from rigid polytetrafluoroethylene, was filled with $FeCl_3$ solution without purging the dissolved oxygen.

All experiments were carried out on an Electronic Universal Testing Machine controlled by computer. Two resistance strain gages were stocked on the chalcopyrite sample surface in the axial and lateral directions, respectively. Using the dynamic–static strain testing system, the axial stress, axial strain and lateral strain were all measured. For comparison, rapid and continuously varying axial stresses (0 Pa; 2×10^5 Pa; 4×10^5 Pa; 6×10^5 Pa) were applied in the electrode potential, polarisation curve and electrical impedance spectroscopy experiments. The experiments were conducted using a stationary electrode in an air-conditioned room at 25 ± 1 °C.

2.2. Stress-electrode potential experiments

An Agilent 34410A high-precision digital multimeter connected to a computer was used to measure the electrode potential. The chalcopyrite electrode and saturated calomel electrode (SCE) through a Luggin capillary salt bridge comprised a standard two-electrode system. The electrode was placed into a rigid Polytetrafluoroethylene cell (60 ml capacity) filled with $FeCl_3$ solution; the chalcopyrite had an exposed area of 4 cm^2. All potentials recorded in this study were relative to the SCE. The experimental arrangement is shown schematically in Fig. 1.

2.3. Stress-polarisation curve experiments

The polarisation curve measurements were performed with a Parstat-2263 equipped with a PowerSuite system. The working

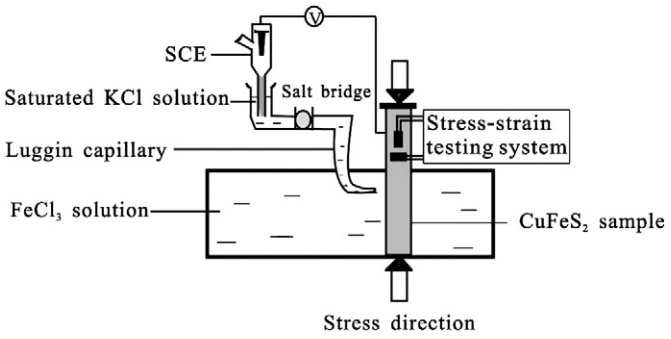

Fig. 1. Scheme of the experimental arrangement.

electrode was the studied chalcopyrite with an exposed area of 4 cm^2, and the counter and reference electrodes were a platinum electrode and the SCE, respectively. The potentials are quoted with respect to the latter.

The polarisation scan was from −250 mV versus an open circuit potential (E_{OC}) to +250 mV versus E_{OC} at a rate of 1 mV/s. The data were recorded after 30 min of immersion in $FeCl_3$ electrolyte solution. The experimental controls and data analysis were carried out using the PowerCorr software offered by Parstat Princeton Applied Research (PAR).

2.4. Stress-electrical impedance spectroscopy experiments

The electrochemical impedance spectroscopy (EIS) measurements were carried out at open circuit potential in the 1×10^5 Hz to 0.01 Hz frequency range, using a Parstat-2263 interfaced to a PC. The amplitude of the sinusoidal voltage was 5 mV·rms. The data were recorded after 1 h of immersion in the working solution. The equivalent circuit model fitting for the AC impedance was evaluated by employing the ZSimpWin (Version 3.10) software from PAR.

3. Results and discussion

3.1. Stress, strain and electrode potential

Fig. 2 presents the electrode potential of chalcopyrite in $FeCl_3$ solution ($0.0010\ mol\cdot L^{-1}$; $0.010\ mol\cdot L^{-1}$; $0.10\ mol\cdot L^{-1}$) under rapid, continuously varying differential stresses. These results demonstrate that the electrode potential of chalcopyrite varied in the different concentrations of $FeCl_3$ solution under similar differential stresses. The electrode potential differences due to the differential stresses were similar across the different solution concentrations. Combining the stresses offered by the Electronic Universal Testing Machine and the chalcopyrite strains measured by dynamic–static strain testing system, we derived a stress–strain–potential difference chart (Fig. 3). From Fig. 3 we can see that the axial stress versus the axial strain and the axial stress versus the lateral strain had positive linear relationships; they obey Hooke's law. These results indicate that the axial stresses acting on the chalcopyrite were elastic stresses, and the chalcopyrite had an elastic deformation. On the other hand, the axial stress and the chalcopyrite potential had a negative linear relationship.

If we define the chalcopyrite potential as $\varphi_H^{CuFeS_2}$, then when the chalcopyrite is under elastic stress conditions, mechanical elements do not affect the electrolyte solution. The chemical potential of reducible ions in solution will not change, although the chemical potential of the chalcopyrite will change. We can deduce that the electrode potential difference for stress is $\Delta\varphi_H^{CuFeS_2} = -\frac{VdP}{ZF}$ (Liu et al., 2009), where V is the chalcopyrite molar volume, Z is the electron transfer number, and F is the Faraday constant. This equation demonstrates that there is a negative linear relation between the

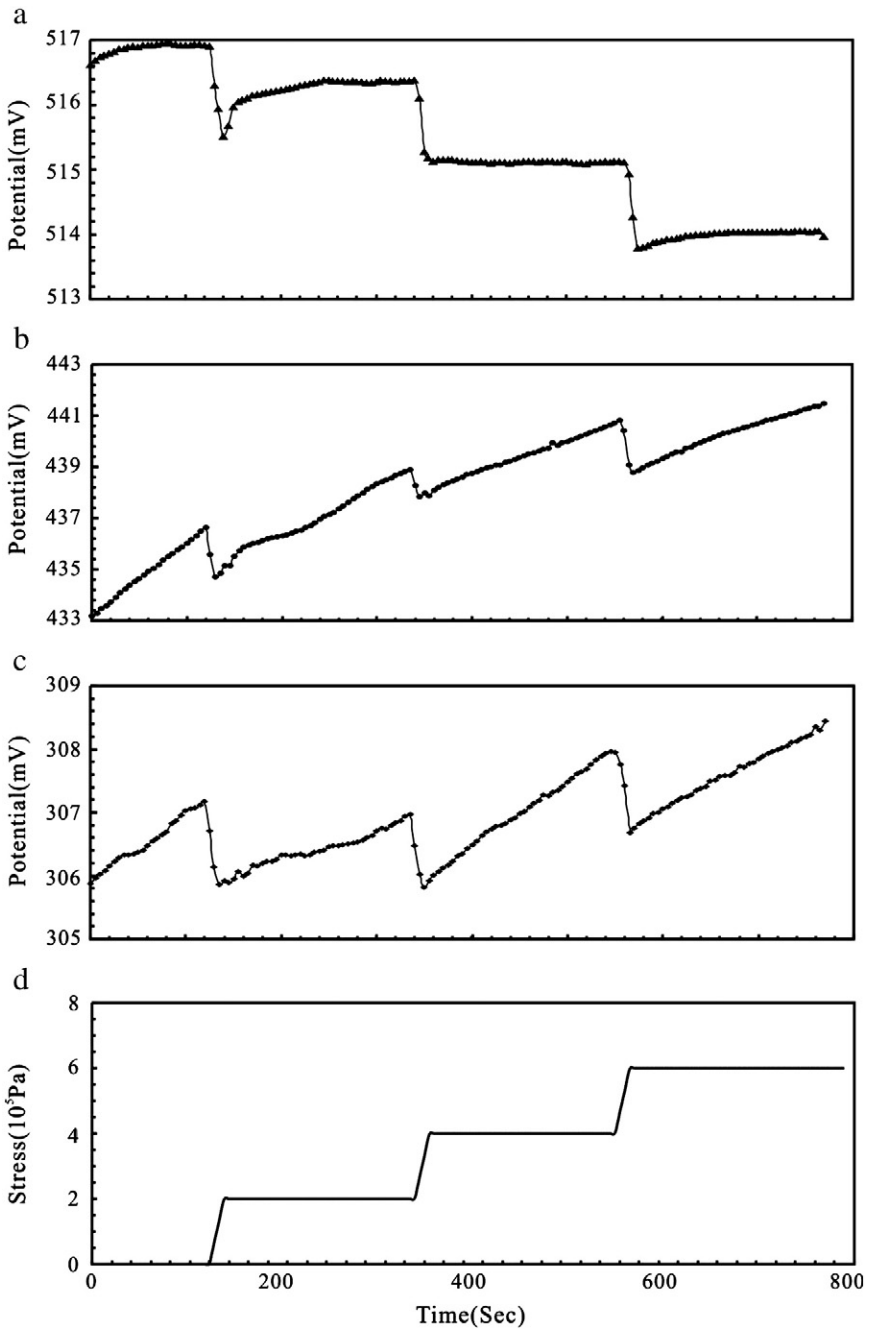

Fig. 2. Variations in chalcopyrite electrode potential under rapid, continuously varying axial stresses (d) in different concentrations $FeCl_3$ solution. (a) 0.10 mol/L, (b) 0.010 mol/L and (c) 0.0010 mol/L.

chalcopyrite potential difference and the stress action. The experimental results shown in Figs. 2 and 3 are consistent with this electrochemical theory.

3.2. Polarisation curves

The Tafel measurements were used to study the corrosion behaviour of the chalcopyrite electrode in contact with a naturally aerated $FeCl_3$ solution ($0.0010\ mol\cdot L^{-1}$; $0.010\ mol\cdot L^{-1}$; $0.10\ mol\cdot L^{-1}$) under rapid and continuously varying elastic axial stresses (0 Pa; 2×10^5 Pa; 4×10^5 Pa; 6×10^5 Pa). The data were recorded after a 30 min immersion in the $FeCl_3$ solution. The Tafel plots are illustrated in Figs. 4-6. By comparing the three figures, we found that, in the same solution concentration with increasing stress, the anode curve shape became steeper and the whole curve obviously shifted in the negative direction along the vertical axis. Under the same stress with an increasing $FeCl_3$ solution concentration, the Tafel curves obviously shifted to the right and became more positive in both the x and y directions. Through the Tafel extrapolation, the corrosion potential (E_{corr}) and corrosion current density (i_{corr}) of the chalcopyrite electrode under differential stresses were obtained, which are listed in Table 1. These data demonstrate that, with increasing stress, the chalcopyrite corrosion current density increased, and the corrosion potential became more negative. This is because stress causes a conversion of the strain energy into electrochemical energy, which thereby changes the electrode potential as 3.1 elaborated, and furthermore has a major influence on the galvanic corrosion of sulphide minerals. However, as the $FeCl_3$ solution concentration increased, the chalcopyrite corrosion current density increased, and the corrosion potential became more positive. These conclusions are further supported by the following EIS experiments.

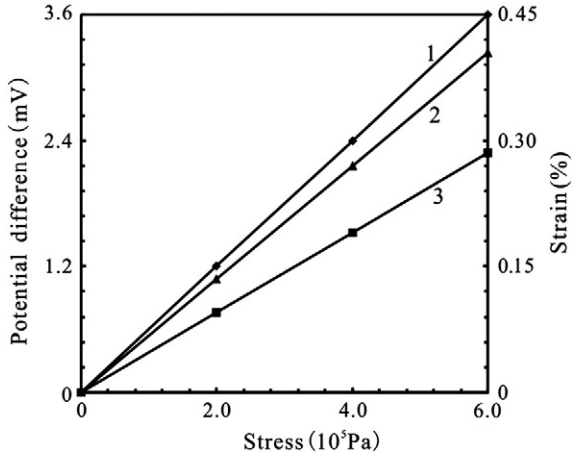

Fig. 3. Chart of chalcopyrite potential difference–stress–strain. (1) axial stress–chalcopyrite potential difference, (2) axial stress–axial strain and (3) axial stress–lateral strain.

3.3. Electrical impedance spectroscopy

Electrical impedance spectroscopy measurements are often used to obtain information about the properties of systems such as the presence of defects, the reactivity of the interface, adhesion, barrier properties, etc. Knowledge of these parameters is very useful for predicting corrosive behaviour (Bonora et al., 1996). In this work, EIS was used to study the micro-kinetic parameters of the covering layer and double-layer, including the charge transfer and double-layer capacitance, of the chalcopyrite electrode in contact with a naturally aerated $FeCl_3$ solution (0.0010 mol·L^{-1}; 0.010 mol·L^{-1}; 0.10 mol·L^{-1}) under rapid and continuously varying elastic axial stresses (0 Pa; 2×10^5 Pa; 4×10^5 Pa; 6×10^5 Pa). The data collection was performed after 1 h of stabilisation time.

The impedance spectra for chalcopyrite obtained in the 0.0010 mol·L^{-1} $FeCl_3$ solution under different elastic axial stresses are presented as Bode plots in Fig. 7a and as a Nyquist diagram in Fig. 7b. The spectra may be described by a simple equivalent circuit model, as shown in Fig. 7c. This model contains a solution resistance (R_s), in series with the parallel network of the charge transfer resistance (R_t), and a constant phase element (CPE) substituted for the double-layer capacitance. The impedance is shown as $Z_{CPE}=[Y_0(j\omega)^n]^{-1}$(Cole, 1941), where Y_0 is the capacitance parameter, j is the imaginary constant, and n is the parameter that characterises the deviation of the system from the ideal capacitive ($n=1$). The parameters R_s, Y_0, n and R_t are shown in Table 2. The impedance parameters listed in Table 2 suggest that stress has an important effect

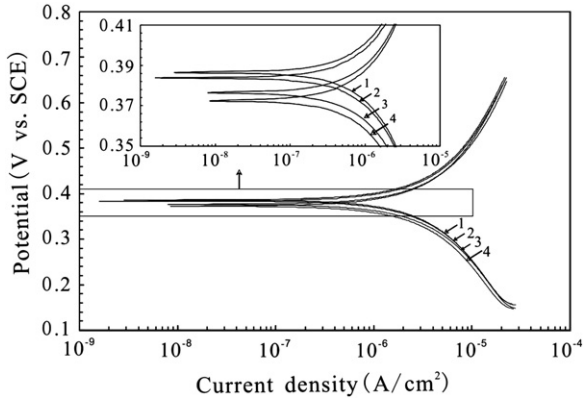

Fig. 5. Tafel plots for chalcopyrite electrode in 0.010 mol·L^{-1} $FeCl_3$ solutions under differential stresses. (1) 0 Pa, (2) 2×10^5 Pa, (3) 4×10^5 Pa and (4) 6×10^5 Pa.

on the chalcopyrite electrode behaviour. As the stress increased from 0 Pa to 6×10^5 Pa, the charge transfer resistance R_t decreased from 12,510 Ω·cm^2 to 8134 Ω·cm^2. The large values of R_t here may be due to two causes: first, XRD measurement discovered that there exist a small of amount of mica and mullite; second, the sulphur film (S^0) covered the electrode surface. The capacitance parameter Y_0 decreased from 0.0007416 S·cm^{-2}·s^{-n} to 0.0007078 S·cm^{-2}·s^{-n}, and the exponent n ranged from 0.3978 to 0.4411.

Fig. 8a presents the Bode plots for the chalcopyrite electrode in the 0.010 mol·L^{-1} $FeCl_3$ solution under different elastic axial stresses. Two time constants can clearly be observed by the two obviously distorted capacitive loops; these can be seen from the Nyquist diagram also (Fig. 8b). The EIS spectra were well fitted with the Randles equivalent electrical circuit (Fig. 8c), where R_s is the solution resistance, R_t is the charge transfer resistance, W is the Warburg diffusion resistance, and a constant phase element (CPE) was substituted for the double-layer capacitance connection of the Helmholtz layer and the surface film. The values of these parameters are tabulated in Table 3. As the stress increased from 0 Pa to 6×10^5 Pa, the charge transfer resistance R_t decreased from 1987 Ω·cm^2 to 1556 Ω·cm^2, and the capacitance parameter Y_0 decreased from 0.001089 S·cm^{-2}·s^{-n} to 0.009905 S·cm^{-2}·s^{-n}. The exponent n ranged between 0.4702 and 0.4994, where a value of n near 0.5 indicates that the inner cell is in concentration polarisation, and the limiting step may be a diffusion process.

According to Fig. 8, we concluded that the first time constant in the high frequency region was a fast charge transfer process between chalcopyrite and the Fe^{3+} species. The second time constant in the low frequency region resulted from the diffusion of anion vacancies

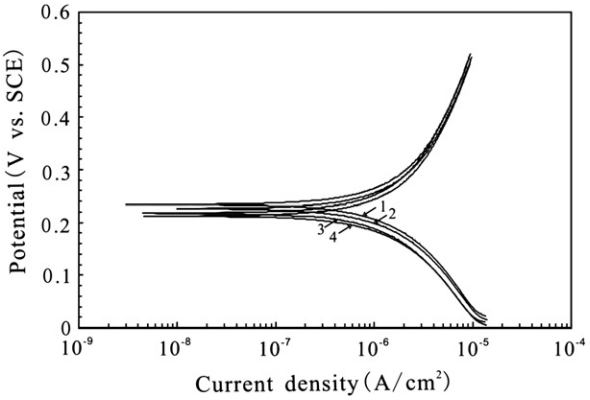

Fig. 4. Tafel plots for chalcopyrite electrode in 0.0010 mol·L^{-1} $FeCl_3$ solutions under differential stresses. (1) 0 Pa, (2) 2×10^5 Pa, (3) 4×10^5 Pa and (4) 6×10^5 Pa.

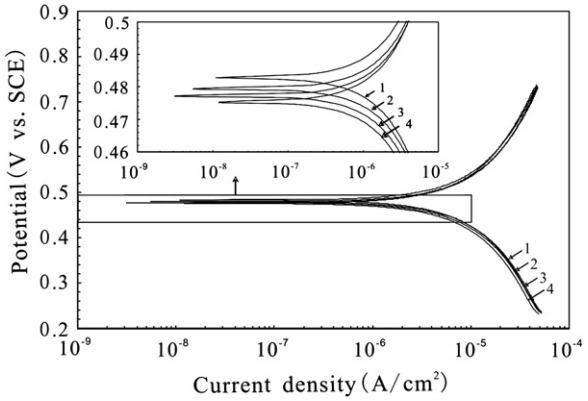

Fig. 6. Tafel plots for chalcopyrite electrode in 0.10 mol·L^{-1} $FeCl_3$ solutions under differential stresses. (1) 0 Pa, (2) 2×10^5 Pa, (3) 4×10^5 Pa and (4) 6×10^5 Pa.

Table 1
Electrochemical corrosion parameters of the $CuFeS_2$ samples from Tafel tests.

$FeCl_3$ ($mol \cdot L^{-1}$)	Stress(10^5 Pa)	E_{corr}(mV)	i_{corr}($\mu A \cdot cm^{-2}$)
0.0010	0	238.4	11.93
	2	236.7	12.09
	4	235.1	12.14
	6	234.1	13.54
0.010	0	373.7	27.85
	2	372.6	27.92
	4	370.9	28.04
	6	368.7	28.76
0.10	0	484.5	102.4
	2	482.9	110.4
	4	481.5	116.3
	6	480.3	126.2

Table 2
Impedance parameters of $CuFeS_2$ in 0.0010 M $FeCl_3$ solutions under differential stresses.

$FeCl_3$ ($mol \cdot L^{-1}$)	Stress (10^5 Pa)	R_s ($\Omega \cdot cm^2$)	CPE, Y_0 ($S \cdot cm^{-2} \cdot s^{-n}$)	n	R_t ($\Omega \cdot cm^2$)
0.0010	0	2719	0.0007416	0.3978	12,510
	2	2808	0.0007353	0.4038	10,370
	4	2705	0.000722	0.4182	8800
	6	2670	0.0007078	0.4411	8134

generated at the chalcopyrite-film interface across the growing S^0 film and their consumption at the film-solution interface.

Fig. 9b presents the Bode plots and a typical Nyquist diagram for the chalcopyrite electrode in the 0.010 $mol \cdot L^{-1}$ $FeCl_3$ solution under different elastic axial stresses. At the lowest frequencies, the phase angle deviated from the line approaching 0^0, and there was a linear dependence of |Z| against the frequency with a slope close to 0.5. This feature shows that the Faradaic process is under mass transfer control and the mass transport occurring across the phase layer or in the electrolyte solution must be taken into account. Therefore, we used in Fig. 9c an equivalent electrical circuit to fit the experimental data. This circuit consists of a solution resistance, R_s, in a series connection with two time constants. The first time constant in the high frequency region was the fast charge transfer process between chalcopyrite and the Fe^{3+} species, where R_t was the charge transfer resistance, and a constant phase element (CPE) was substituted for the double-layer capacitance connection of the Helmholtz layer and the surface film. The second time constant in the low frequency region resulted from the diffusion of the point defects across the growing sulphide film on the chalcopyrite surface, the metallographic microscope results proved this. The Warburg element *O* used in the circuit represented the dimensional diffusion through a layer of finite thickness. From the electrical point of view, *O* is equivalent to the impedance of a finite-length transmission line and is characterised by two parameters, an "admittance" parameter, Y_o, and a "time constant" parameter, *B*. Y_o has the same definition as for the Warburg impedance. If the thickness of the film is δ, and the diffusion coefficient is D, then the constant *B* can be expressed as $B = \delta/\sqrt{D}$. *B* characterises the time it takes for a reactant to diffuse through the thin film.

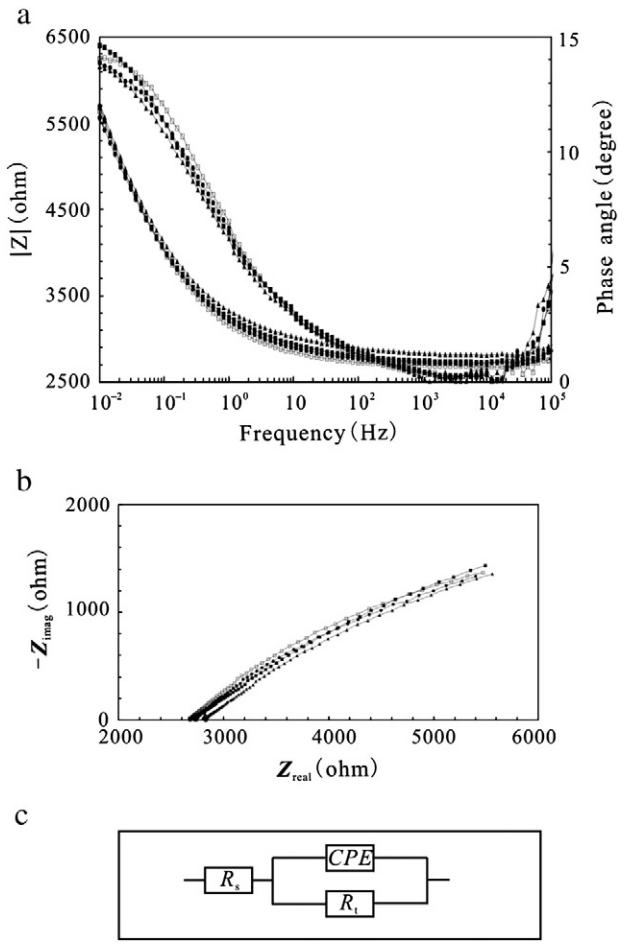

Fig. 7. Bode plots and phase angles (a), Nyquist impedance spectra (b) and equivalent circuit (c) for chalcopyrite under differential stresses in 0.0010 $mol \cdot L^{-1}$ $FeCl_3$ solutions. (■) 0 Pa, (▲) 2×10^5 Pa, (●) 4×10^5 Pa and (□) 6×10^5 Pa.

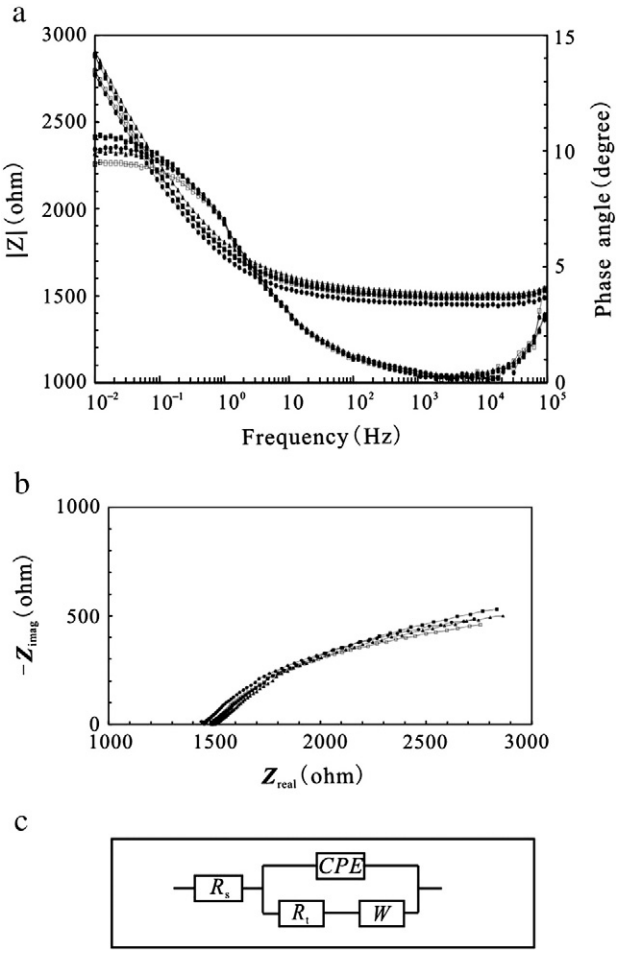

Fig. 8. Bode plots and phase angles (a), Nyquist impedance spectra (b) and equivalent circuit (c) for chalcopyrite under differential stresses in 0.010 $mol \cdot L^{-1}$ $FeCl_3$ solutions. (■) 0 Pa, (▲) 2×10^5 Pa, (●) 4×10^5 Pa and (□) 6×10^5 Pa.

Table 3
Impedance parameters of $CuFeS_2$ in 0.010 M $FeCl_3$ solutions under differential stresses.

$FeCl_3$ ($mol \cdot L^{-1}$)	Stress (10^5 Pa)	R_s ($\Omega \cdot cm^2$)	CPE, Y_0 ($S \cdot cm^{-2} \cdot s^{-n}$)	n	R_t ($\Omega \cdot cm^2$)	W, Y_0 ($S \cdot cm^{-2} \cdot s^{-0.5}$)
0.0010	0	1485	0.001089	0.4702	1987	0.008678
	2	1508	0.001001	0.4722	1887	0.009393
	4	1447	0.0009934	0.4922	1657	0.008530
	6	1485	0.0009905	0.4994	1556	0.009118

The fit parameters obtained for different elastic axial stresses of film formation are contained in Table 4. With the stress increasing from 0 Pa to 6×10^5 Pa, the charge transfer resistance R_t decreased from 352.5 $\Omega \cdot cm^2$ to 248.6 $\Omega \cdot cm^2$, the capacitance parameter *CPE* Y_0 decreased from 0.003618 $S \cdot cm^{-2} \cdot s^{-n}$ to 0.002785 $S \cdot cm^{-2} \cdot s^{-n}$, the exponent n ranged from 0.3415 to 0.3985, the capacitance parameter coth Y_0 increased from 0.01932 $S \cdot cm^{-2} \cdot s^{-n}$ to 0.03461 $S \cdot cm^{-2} \cdot s^{-n}$, and the time constant B decreased from 4.952 $s^{-0.5}$ to 4.033 $s^{-0.5}$. The results indicated that the dimensional diffusion layer decreased, its capacitance increased, and the time that ions diffused through the thin film decreased with the increasing stress.

By comparing the above experiments, we can see that, in any concentration of $FeCl_3$ solution, the charge transfer resistance and the capacitance parameter Y_0 always decreased with increasing elastic axial stresses. The charge transfer resistance represents the electrode polarisation resistance, and its value represents the ease of the electron transfer on the electrode surface; the capacitance parameter Y_0 represents the electric double-layer at the mineral-water interface, and its value characterises the ease of diffusion of ions between the electric double-layers. At room temperature and 1 atm, the dissolved O_2 was very low (8.0–8.5 mg/L), especially because Fe^{3+} is a strongly oxidising ion, so in these experiments the influence of dissolved oxygen on galvanic corrosion can be neglected. The electrode reaction is expressed as follows (Holmes and Crundwell, 2000):

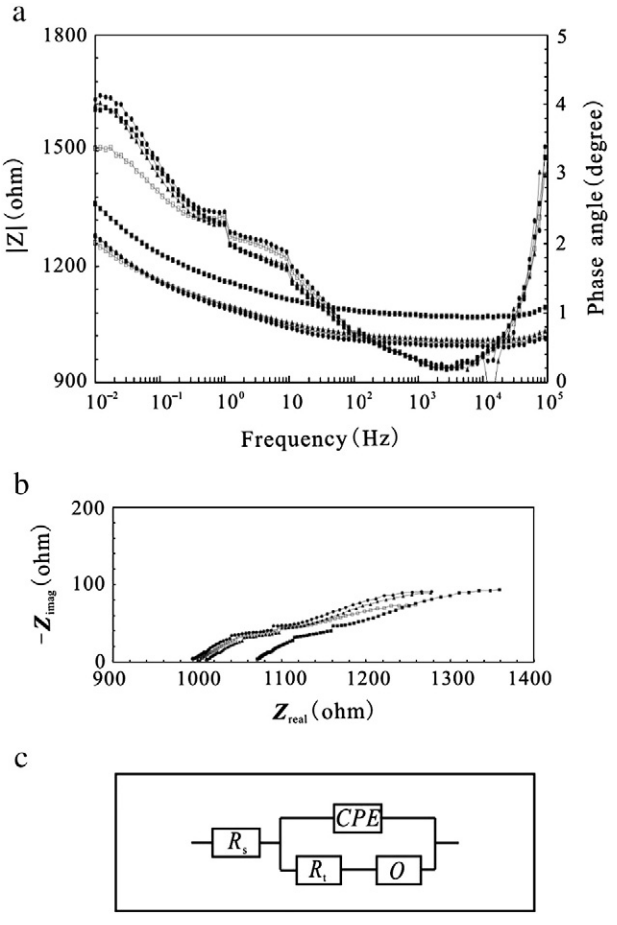

Fig. 9. Bode plots and phase angles (a), Nyquist impedance spectra (b) and equivalent circuit (c) for chalcopyrite under differential stresses in 0.10 $mol \cdot L^{-1}$ $FeCl_3$ solutions. (■) 0 Pa, (▲) 2×10^5 Pa, (●) 4×10^5 Pa and (□) 6×10^5 Pa.

$$\text{Anode}: CuFeS_2 \rightarrow Cu^{2+} + Fe^{2+} + 2S^0 + 4e^- \quad (1)$$

$$\text{Cathode}: Fe^{3+} + e^- \rightarrow Fe^{2+} \quad (2)$$

When the elastic axial stresses increased, the chalcopyrite electrode gained more stain energy, which then changed into electrochemical energy, so electron transfer on the electrode surface became easier, i.e., the charge transfer resistance R_t decreased. Similarly, under this condition, the ion diffusion should be changed more easily, i.e., the capacitance parameter Y_0 should increase, but the experiments yielded the opposite results. This conflict maybe due to the following causes: the chalcopyrite sample surface has a small amount of mica and mullite; though these elements did not impair the electrode action, they may have adsorbed ions. With the increasing stress, the mica and mullite crystal lattice would have become more compact, causing the ion diffusion to be more difficult; On the other hand, as the amount of sulphur on the surface increases, it becomes more difficult for Fe^{2+} ions to diffuse, and a high concentration of Fe^{2+} ions remains at the mineral surface. Part of the Fe^{2+} is oxidised, forming Fe^{3+}. The accumulation of Fe^{2+} can reduce the concentration of protons near the electrode, increasing the local pH and favouring the formation of thiosulphate, as proposed by Paul et al. (1978). The following reactions might occur: $2S^0 + 3H_2O \rightarrow S_2O_3^{2-} + 6H^+ + 4e^-$ and $2FeS + 3H_2O \rightarrow S_2O_3^{2-} + 2Fe^{2+} + 6H^+ + 8e^-$ (Biernat and Robins, 1972). As the stress increased, pitting corrosion became serious, and the above two reactions would become more prominent, resulting in more difficult ion diffusion.

3.4. Implications

From the above experiments, we found that differential stress markedly affects the sulphide mineral electrode potential and consequently affects the sulphide mineral electrochemical behaviour. Thus these stresses must ultimately affect hydrometallurgy and mineral processing (Baláž, et al., 2004). In these fields, the use of high-energy mills allows a dramatic change of the structure and surface properties of solids to be induced (Baláž, 2000, Tkacova, 1989). The stress relaxation cause changes in the reactivity of the solid substance, the so-called mechanical activation (Boldyrev and Tkacova, 2000). The active mechanical energy is partially transferred to the particles; its effects include a multitude of elementary physicochemical micro- and macro-processes. The mechanical energy leads to changes of the material structure and to the occurrence of structural defects such as changes of the surface, lattice distortion and the conversion of long-range order to short-range order (Baláž, 2000; Tkacova, 1989). In our experiment, we found that the mineral electrode potential had a negative linear relationship to the stress action, and its only affects by the mineral electrode itself characters. Thus, if we apply the stress properly, we can broaden the difference between the potentials of the two different minerals and then easily separate them.

4. Conclusions

The electrochemical behaviour of chalcopyrite ($CuFeS_2$) in $FeCl_3$ solution under differential stress has been studied using polarisation

Table 4
Impedance parameters of $CuFeS_2$ in 0.10 $FeCl_3$ solutions under differential stresses.

$FeCl_3$ ($mol \cdot L^{-1}$)	Stress (10^5 Pa)	R_s ($\Omega \cdot cm^2$)	CPE,Y_0 ($S \cdot cm^{-2} \cdot s^{-n}$)	n	R_t ($\Omega \cdot cm^2$)	Coth, Y_o ($S \cdot cm^{-2} \cdot s^{-0.5}$)	B ($s^{-0.5}$)
0.10	0	1062	0.003618	0.3415	352.5	0.01932	4.952
	2	1002	0.003470	0.3483	295.4	0.02258	4.633
	4	987.8	0.002812	0.3889	262.4	0.02316	4.571
	6	996.8	0.002785	0.3985	248.6	0.03461	4.033

curves and electrical impedance spectroscopy. Several conclusions can be drawn from this research:

(1) There is a negative linear relation between the chalcopyrite potential difference and the stress action. The mathematical expression is:

$$\Delta\varphi_H^{CuFe_2} = -\frac{VdP}{ZF}$$

(2) Without changes to other conditions, increased differential stress lead to a higher corrosion current density and a more negative corrosion potential. Stress causes a conversion of the strain energy into electrochemical energy, which thereby increases the activation energy, and speeds up the corrosion electrochemical behaviour.

(3) EIS experiments indicated that, in various concentrations of $FeCl_3$ solutions ($0.0010\ mol \cdot L^{-1}$, $0.010\ mol \cdot L^{-1}$ and $0.10\ mol \cdot L^{-1}$) in the stress experiments, there were different micro-reaction mechanisms and the electrical equivalent circuit can be interpreted from simple, Randles and point defect model, respectively. Without changes to other conditions, increasing the differential stress decreased the charge transfer resistance and increased the Warburg diffusion capacitance. The results explain why increasing stress causes the chalcopyrite corrosion electrochemical behaviour to increase.

Acknowledgments

Many thanks should be extended to H.G. Xu and M.Q. Yang for their technical assistance in the experimental work. This work was financially supported by the National Natural Science Foundation of China (40803017; 40573046), the Large-scale Scientific Apparatus Development Program of Chinese Academy of Sciences (YZ200720), the Municipal Science and Technology Foundation of Guizhou Province, China (No. 2008GZ02240), and the West Light Foundation Doctor Cultivate Progress Foundation of the Chinese Academy of Sciences.

References

Arce, E.M., González, I., 2002. A comparative study of electrochemical behavior of chalcopyrite, chalcocite and bornite in sulfuric acid solution. Int. J. Miner. Process. 67, 17–28.

Baláž, P., 2000. Extractive metallurgy of activated minerals, first ed. Elsevier, Amsterdam.

Baláž, P., Takacs, L., Luxová, M., Godočíková, E., Ficeriová, J., 2004. Mechanochemical processing of sulphidic minerals. Int. J. Miner. Process. 74, 365–371.

Biernat, R.J., Robins, R.G., 1972. High-temperature potential/pH diagrams for the iron–water and iron–water–sulphur systems. Electrochem. Acta 17, 1261–1283.

Boldyrev, V.V., Tkacova, K., 2000. Mechanochemistry of solids: past, present, and prospects. J. Mater. Synth. Process. 8, 121–132.

Bonora, P.L., Deflorian, F., Fedrizzi, L., 1996. Electrochemical impedance spectroscopy as a tool for investigating underpaint corrosion. Electrochem. Acta. 41, 1073–1082.

Dutrizac, J.E., MacDonald, R.J.C., 1973. The effect of some impurities on the rate of chalcopyrite dissolution. Can. Metall. Q. 12 (4), 409–420.

Dutrizac, J.E., 1981. The dissolution of chalcopyrite in ferric sulfate and ferric chloride media. Metall. Trans. B 12, 371–378.

Dutrizac, J.E., 1992. The leaching of sulphide minerals in chloride media. Hydrometall. 29, 1–45.

Farquhar, M.L., Wincott, P.L., Wogelius, R.A., Vaughan, D.J., 2003. Electrochemical oxidation of the chalcopyrite surface: an XPS and AFM study in solution at pH 4. Appl. Surf. Sci. 218, 34–43.

Gonzalo, V.G., Berny, F.R., Dixon, D.G., 2007. The active–passive behavior of chalcopyrite. J. Electrochem. Soc. 154, 299–311.

Hackl, R.P., Dreisinger, D.B., Peters, E., King, J.A., 1995. Passivation of chalcopyrite during oxidative leaching in sulphate media. Hydrometall. 39, 25–48.

Havlík, T., Milan Škrobian, M., Baláž, P., Kammel, R., 1995. Leaching of chalcopyrite concentrate with ferric chloride. Int. J. Miner. Process. 43, 61–72.

Hiroyoshi, N., Arai, M., Miki, H., Tsunekawa, M., Hirajima, T., 2002. A new reaction model for the catalytic effect of silver ions on chalcopyrite leaching in sulfuric acid solutions. Hydrometall. 63, 257–267.

Holmes, P.R., Crundwell, F.K., 2000. The kinetics of the oxidation of chalcopyrite by ferric ions and dissolved oxygen: an electrochemical study. Geochim. Cosmochim. Acta 64 (2), 263–274.

Lázaro, I., MartÍnez-Medina, N., Rodríguez, I., Arce, E., González, I., 1995. The use of carbon paste electrodes with non-conducting binder for the study of minerals: chalcopyrite. Hydrometall 38, 277–287.

Liu, Q.Y., Li, H.P., Zhou, L., 2009. Experimental study of chalcopyrite-galena galvanic in a flowing system and its applied implications. Hydrometall. 96, 132–139.

Lu, Z.Y., Jeffrey, M.I., Lawson, F., 2000. An electrochemical study of the effect of chloride ions on the dissolution of chalcopyrite in acidic solutions. Hydrometall. 56, 145–155.

Munoz, P.B., Miller, J.D., Wadsworth, M.E., 1979. Reaction mechanism for the acid ferric leaching of chalcopyrite. Metall. Trans. B 10, 149–158.

Paul, R.L., Nicol, M.J., Diggle, J.W., Saunders, A.P., 1978. The electrochemical behaviour of galena (lead sulphide) — I. Anodic dissolution. Electrochem. Acta 23 (7), 625–633.

Price, D.C., Chilton, J.P., 1980. The electroleaching of bornite and chalcopyrite. Hydrometall. 5, 381–394.

Tkacova, K., 1989. Mechanical activation of minerals, first ed. Elsevier, Amesterdam.

Vaughan, D.J., England, K.E.R., Kelsall, G.H., Yin, Q., 1995. Electrochemical oxidation of chalcopyrite ($CuFeS_2$) and the related metal-enriched derivatives $Cu_4Fe_5S_8$, $Cu_9Fe_9S_{16}$, and $Cu_9Fe_8S_{16}$. Am. Mineralog. 80, 725–731.

Velásquez, P., GÓmez, H., Leinen, D., Ramos-Barrado, J.R., 1998. Electrochemical impedance spectroscopy analysis of chalcopyrite $CuFeS_2$ electrodes. Colloids Surf., A 140 (1–3), 177–182.